Phase field crystal study of the crystallization modes within the two-phase region*

Yang Tao(杨 涛)†, Zhang Jing(张 静), Long Jian(龙 建), Long Qing-Hua(龙清华), and Chen Zheng(陈 铮)

State Key Laboratory of Solidification Processing, Northwestern Polytechnical University (NPU), Xi'an 710072, *China*

(Received 13 December 2013; revised manuscript received 18 January 2014; published online 10 June 2014)

Using the phase field crystal approach, the crystallization process within the liquid–solid coexistence region is investigated for a square lattice on an atomic scale. Two competing growth modes, i.e., the diffusion-controlled growth through long-range atomic migration in liquid and the diffusionless growth through local atom rearrangement, which give rise to two completely different crystallization behaviors, are compared. In the diffusion-controlled regime, the interface migrates in a layerwise manner, leading to a gradual change of crystal morphology from truncated square to four-fold symmetric dendrite with the increase of driving force. For the diffusionless growth mode, a single crystal with no significant density change occupies the whole system at a faster rate while exhibiting a small growth anisotropy. The competition between these two modes is also discussed from the key input of the phase field crystal model: the correlation function.

Keywords: phase field crystal, diffusion-controlled, diffusionless, dendrite

PACS: 81.10.Fq, 64.70.dg, 61.50.Ah, 07.05.Tp **DOI:** 10.1088/1674-1056/23/8/088109

1. Introduction

At the heart of material properties lie diverse microstructures which are closely related to various crystallization processes. Therefore, exploring the relationship between the crystallization process and its consequential morphology constitutes an indispensible part in the project of material science fabrication. Normally, a progressive change in crystal morphology from the symmetric single crystal to branching dendrites, followed by the polycrystalline structure is expected with the variation of the driving force for crystallization, which proceeds with the well-known diffusion-controlled or slow growth mode.[1] However, another theoretically unanticipated morphological transition between symmetric and irregular-shaped single crystal has been indicated in both colloidal and polymeric materials by recent work.[2,3] Besides rationalizing this phenomenon from the aspect of the dynamical reduction in the growth anisotropy,[4] the competition of a newly discovered growth mode, termed as the diffusionless or fast growth mode, together with the diffusion-controlled mode, is proposed to account for the formation of the irregular, fractal-like mesopatterns.[5,6] The diffusionless growth mode in which the crystalline ordering takes place without an appreciable density change occurs under a high driving force.[7,8] Gaining a deeper insight into these two growth modes and their associated various crystal morphologies would greatly facilitate the advancement of solidification technology. Based on gradient thermodynamics,[9,10] the phase field approach has been used widely in computer simulations for both diffusional and diffusionless transformations.[11–18] Recently, a new modeling paradigm, the phase field crystal model (PFC), has emerged and been formulated according to the classical density functional theory,[19] and its grand potential has been demonstrated by numerous applications, spreading over grain boundaries,[20–22] solid-state transformations,[23] and atomic attachment kinetics in crystallization.[24–26] The quintessential advantage of the PFC approach lies in its integration of small length scale with diffusive dynamics. It is the PFC model by which the coupling of crystallization modes and morphological transitions has been theoretically discovered.[8] However, due to the intrinsic restriction on the model they adopted, limited crystal symmetries (only a triangular structure in two dimensions) are available to be investigated.[7,8] With the efforts made by Greenwood *et al*., various crystal symmetries other than triangle structure in two dimensions can be stabilized for the first time in PFC by constructing relevant correlation kernels.[27,28] Variations of crystal properties inherent within different structures exert a great influence on the crystallization process, rendering a further study of other symmetries necessary.

In this paper, the atomic crystallization process occurring in the solid–liquid coexistence region is explored for a square lattice using the PFC method. The two growth modes, diffusion-controlled and diffusionless, with their associated morphological evolution are captured and discussed in our simulation. In addition, the crucial role played by the correlation function in the behaviors of the PFC model is demonstrated[27–29] to directly lead to the presence of various crystal structures.

*Project supported by the National Natural Science Foundation of China (Grant Nos. 51174168 and 51274167) and the Foundation for Fundamental Research of Northwestern Polytechnical University, China (Grant No. JC20120222).

†Corresponding author. E-mail: 420929211@163.com

© 2014 Chinese Physical Society and IOP Publishing Ltd

2. Phase field crystal methodology

The dimensionless free energy functional of the PFC model adopted here is formulated as[27]

$$F = \int \mathrm{d}\boldsymbol{r} \left\{ \frac{\boldsymbol{n}}{2} - \eta \frac{\boldsymbol{n}^3}{6} + \nu \frac{\boldsymbol{n}^4}{12} - \frac{1}{2}\boldsymbol{n} \int \mathrm{d}\boldsymbol{r}' \boldsymbol{C}_2(|\boldsymbol{r}-\boldsymbol{r}'|)\boldsymbol{n}' \right\}, \quad (1)$$

and the free energy dissipation is governed by a conservative dynamics,

$$\frac{\partial \boldsymbol{n}}{\partial t} = \nabla^2 \frac{\delta F}{\delta \boldsymbol{n}}, \quad (2)$$

where $\boldsymbol{n}$ represents the atomic number density, and parameters η and ν are the polynomial expansion coefficients of the ideal energy, with $\eta = \nu = 1$ corresponding to a Taylor series expansion with respect to the reference density. The pair correlation function $\boldsymbol{C}_2(|\boldsymbol{r}-\boldsymbol{r}'|)$ describing two point interactions is constructed in Fourier space using the envelope of the superposition of all relevant peaks of the desired crystal structure defined as[27]

$$\hat{\boldsymbol{C}}_2(\boldsymbol{k})_i = \exp\left(-\frac{\sigma^2 k_i^2}{2\rho_i \beta_i}\right) \exp\left(-\frac{(k-k_i)^2}{2\alpha_i^2}\right), \quad (3)$$

where k_i $(i = 1,2)$ denote the positions of reciprocal space peaks, represented by the Gaussian distribution field with its width α_i $(i = 1,2)$, and σ is linked to the system temperature (for detailed interpretations of other parameters, see Ref. [28]). A stable square lattice is produced with the parameters $k_1 = 1/\sqrt{2}k_2 = 2\pi$, and $\sigma = 0$. Two sets of peak width values are chosen with $\alpha_1 = 3$ and 2 while $\alpha_2 = 1/\sqrt{2}\alpha_1$. Equation (2) is solved in Fourier space using a semi-implicit technique with periodic boundary conditions applied in both directions.[22] A simulation cell is discretized with a grid size $\mathrm{d}x = 0.1$ and time step $\mathrm{d}t = 0.01$ for greater stability and efficiency. The initial condition consists of a centrally-located solid nucleus surrounded by the undercooled liquid. The density field of the predefined nucleus with square symmetry is given by a two-mode approximation: $\boldsymbol{n}(\boldsymbol{r}) = \bar{n} + 2A_1(\cos(q\boldsymbol{x}) + \cos(q\boldsymbol{y})) + 4A_2\cos(q\boldsymbol{x})\cos(q\boldsymbol{y})$, where $\bar{n}$ represents the initial average density of liquid phase. The amplitudes A_i $(i = 1,2)$ and wave number q are determined by the free energy minimization. All simulations are performed within the liquid–solid coexistence region according to Fig. 1.

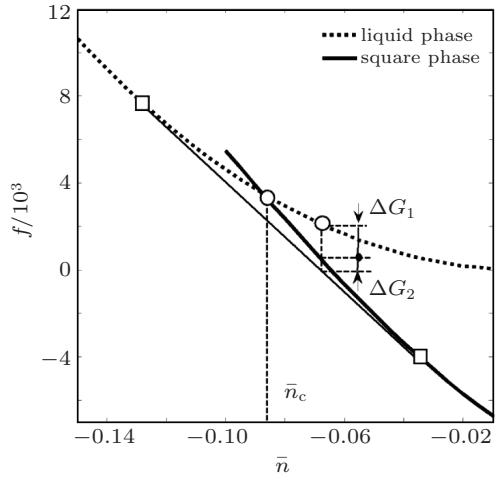


Fig. 1. Free energy curves for liquid (dotted line) and square (bold solid line) phases. The equilibrium densities are denoted by the thin solid line and squares. The point $\bar{n}_c$ represents the average density where two phases have equal free energy density. The free energy difference ΔG_1 denotes the driving force of the diffusionless transformation, while ΔG_2 corresponds to the driving force of its subsequent equilibrium precipitation.

3. Results and discussion

The analytic free energy curves for liquid and solid phases with respect to average number density have been presented using a two-mode approximation, and are shown in Fig. 1. As seen in Figs. 1 and 8, instead of precipitating the equilibrium product phase, a diffusionless phase is formed through the mechanism of vacancy trapping,[8] analogously to the solute trapping of rapid solidification. Diffusionless transformation here is referred to as the process where there is no significant composition change within the product and matrix phase. The occurrence of the above process within a two-phase region must be thermodynamically feasible. As shown in Fig. 1, the energy difference ΔG_1 would serve as the driving force in the diffusionless growth process. For illustrative purposes, driving force hereafter refers to the total or integrated driving force. When the average density moves towards the point $\bar{n}_c$, where the two phases have equal free energy, the corresponding driving force decreases, and eventually reaches zero. Therefore, for a diffusionless transformation to take place the average density should lie beyond the critical point $\bar{n}_c$, similar to that of the massive transformation occurring in the coexistence region.[30] However, it is worthy to note that the thermodynamic driving force for a direct precipitation process, i.e., the sum of ΔG_1 and ΔG_2, is necessarily higher than that of diffusionless transformation ΔG_1. The reason why diffusionless transformation can still be favored is due to the facilitation provided by the absence or reduction of the chemical interfacial energy, which arises from the average density discrepancy between equilibrium phases. So far, the above discussion merely consists of a necessary condition for diffusionless transformation. Moreover, a kinetic criterion also should be fulfilled following the reasoning in Ref. [30], namely the interface migration rate should be high enough to prevent the precipitation of the equilibrium phases at the interface, which happens at a lower growth rate in the diffusion-controlled regime. The above analysis from the perspectives of thermodynamics and kinetics is well demonstrated in our simulation. In Figs. 2(a) and 3, simulated with $\bar{n} = -0.1$ (smaller than $\bar{n}_c$), the crystallization process is governed by the slow growth mode which exhibits a parabolic relationship between the mean radius of the crystal and time. When the average density $\bar{n}$ surpasses the critical value, the crystallization mode is switched to the diffusionless mode as shown in Figs. 2(b) and 8, accompanied with a linear growth rate.

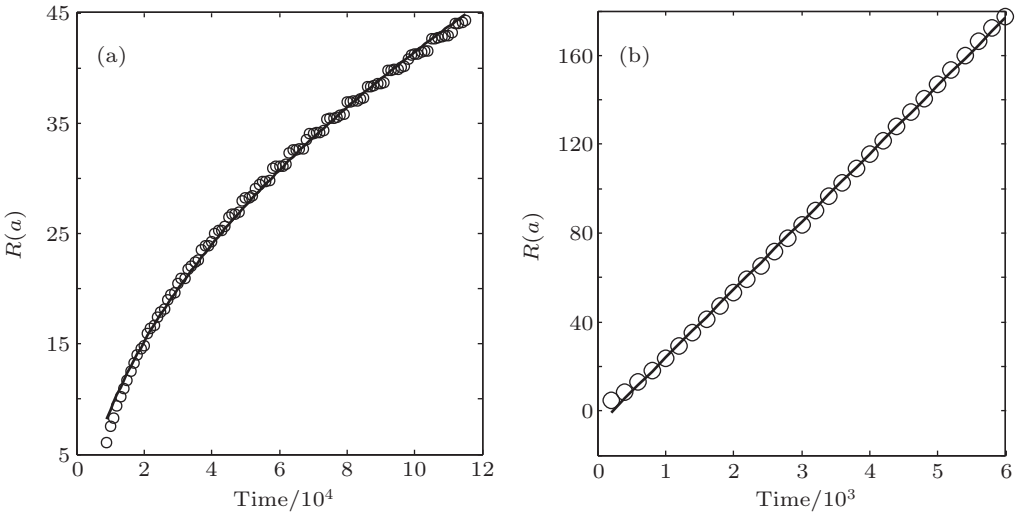


Fig. 2. Plots of the radius of the square crystal versus time with simulation parameters $\bar{n} = -0.1$, $\alpha_1 = 3$ in panel (a) and $\bar{n} = -0.06$, $\alpha_1 = 2$ in panel (b). The solid lines are the best fittings to parabolic and linear growth rates for panels (a) and (b), respectively.

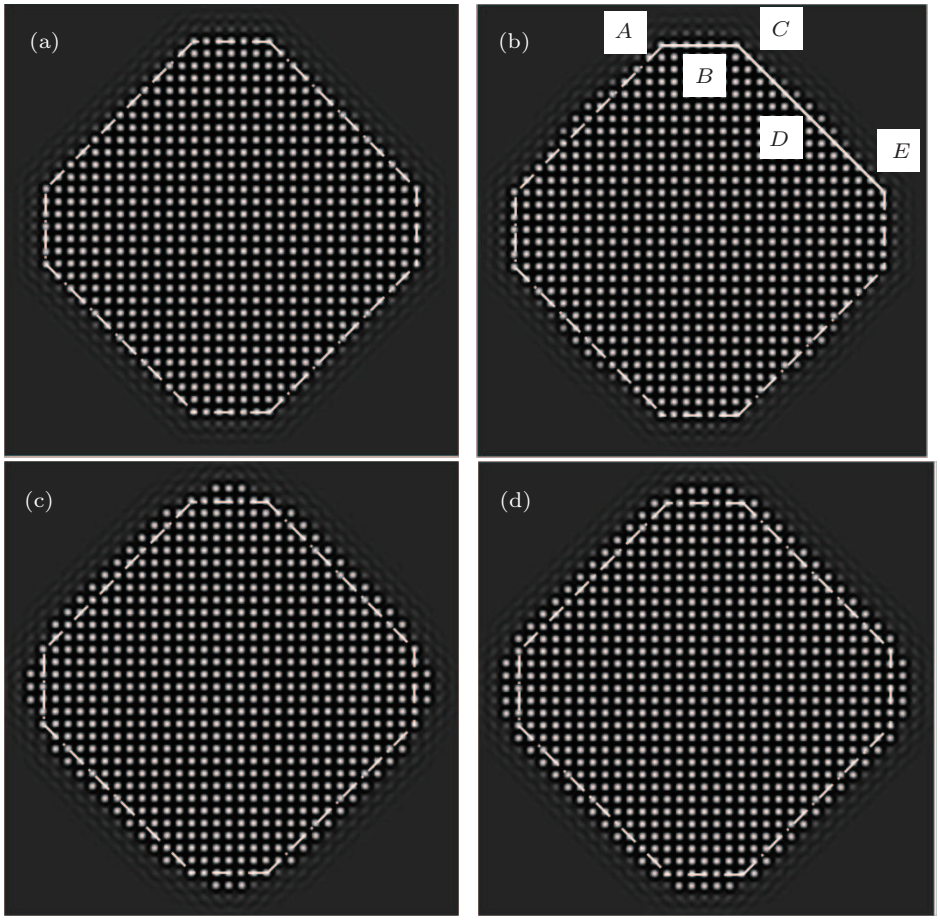


Fig. 3. The diffusion-controlled growth process simulated with $\bar{n} = -0.1$ and $\alpha_1 = 3$, at times: (a) $t = 4.34 \times 10^4$, (b) $t = 4.4 \times 10^4$, (c) $t = 4.5 \times 10^4$, and (d) $t = 4.6 \times 10^4$. The two white solid lines *ABC* and *CDE* indicate the locations of the faces $\{10\}$ and $\{11\}$, respectively.

The diffusion-controlled crystallization process is shown in Fig. 3, with the simulation parameters $\bar{n} = -0.1$ and $\alpha_1 = 3$. As shown in Fig. 3(a), a truncated square-shaped crystal, consisting of 4 $\{11\}$ planes with tips pointing to $\langle 10 \rangle$ direction, is evolved from a sphere-shaped nucleus, which is attributed to the growth rate anisotropy. In the spirit of better visualization, the outermost layer of the crystal before the next nucleation happens is marked in white dashed lines in the following figures as a benchmark. As shown in Fig. 3(b), the nucleation of a new layer takes place first at the center of the $\{11\}$ planes

at $t = 4.4 \times 10^4$. The preferred nucleation sites are then rationalized in terms of free energy density distribution along $\{10\}$ and $\{11\}$ faces, which are corresponding to the white solid lines *ABC* and *CDE* in Fig. 3(b), respectively. The profiles of smoothed free energy density along these two lines are plotted for different times in Fig. 4, obtained by employing a Fourier filter based on Eq. (A1) in Ref. [31]. As figure 4(a) shows, the free energy at the center of the $\{11\}$ faces, position *D*, is much lower than those at the corners, positions *E* and *C*, implying a higher driving force for nucleation at the center than at the corners, and it reaches the minimum at $t = 4.4 \times 10^4$, which indicates the occurrence of nucleation event. As the growth process proceeds, atoms are absorbed into the steps of this newly nucleated $\{11\}$ layer in order to maintain a lower interfacial energy, which leads to the lateral growth along the $\langle 11 \rangle$ direction as depicted in Fig. 3(c). In the mean time, the driving force of position *B* comes to a maximum at time $t = 4.5 \times 10^4$, resulting in another new nucleation event at the center of the existing $\{10\}$ faces as in Fig. 3(c). After this, a lateral attachment of solid atoms along the $\langle 10 \rangle$ direction is followed in the same way as that for $\{11\}$ faces as shown in Fig. 3(d). As a consequence, one layer extension of the crystal into liquid is completed when these two lateral growths meet. Through the repetition of the above processes, the growth process progresses through the layer-by-layer growth mode as described above, which is indicated by the successive jumps of open circles in Fig. 2(a).

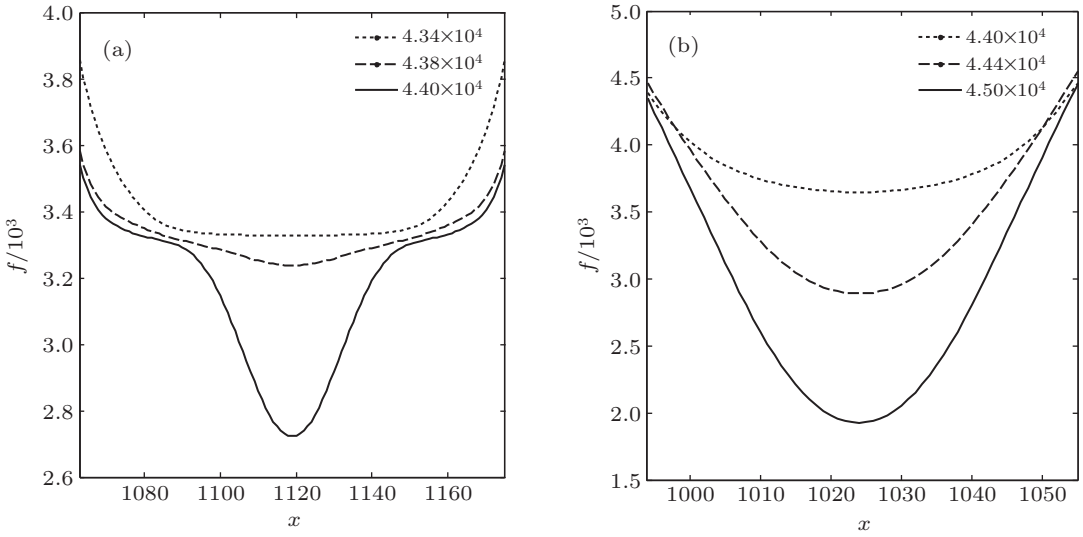


Fig. 4. Smooth free energy distribution along lines *CDE* (a) and *ABC* (b) before and during nucleation in the early growth stage, corresponding to Fig. 3.

It is worthy to note that at later times, the nucleation position of the $\{11\}$ faces transits to the area nearby the corners where the $\{11\}$ and $\{10\}$ faces connect, while the nucleation sites of the $\{10\}$ faces remain unchanged as shown in Fig. 5. In order to obtain a clear atomic resolution, only a quarter of the crystal is displayed. Figure 6 shows the corresponding free energy evolution process along the $\{10\}$ and $\{11\}$ faces for the period right before and during nucleation. As shown in Fig. 6, the smooth free energy density of $\{11\}$ faces now split into two located near the crystal corners, while that of $\{10\}$ faces still stays in the center, which leads to the variation of preferred nucleation sites for these two planes. Conventionally, the preferred nucleation sites would be the area close to the crystal corners caused by the non-uniform distribution of the supersaturation.[32] However, according to the simulation results, it appears that the two preferable nucleation areas near the corners overlap on these faces when the crystal faces are small during the initial stage of growth, resulting in a new maximum supersaturation at the center. Comparing Figs. 3 and 5, the nucleation sites for the $\{10\}$ faces are maintained at the center due to the preservation of their small size, while the transition for $\{11\}$ faces is caused by the increase in length.

As the initial average density of the liquid phase increases, the driving force for the nucleation event goes up as denoted by ΔG_1 in Fig. 1, which leads to a shorter incubation time. Therefore, the stability of layer-by-layer growth would be undermined when the incubation time becomes shorter than the growth time, and eventually the branching dendrite develops.[24] Figure 7 shows the evolution process of the truncated square crystal into four-fold symmetric dendrites, with the simulation parameters $\bar{n} = -0.05$ and $\alpha_1 = 3$. As shown in Fig. 7(a), the layer-by-layer growth mode dictates the early growth regime. In the insets of Figs. 7(a) and 7(b), the corresponding number density profiles are shown for areas enclosed

by the black dashed box, where the growth modes are clearly indicated by the number of partially-filled layers. In the intermediate stage of growth, the multi-layer growth mode is entered when new {11} layers nucleate before the former layers are fully filled, which results in the formation of steps in {11} planes as shown in Fig. 7(b). As the growth process proceeds, branches of the dendrite are gradually formed with more steps generated in the {11} layers, and reaches a steady state after some time as shown in Figs. 7(c) and 7(d).

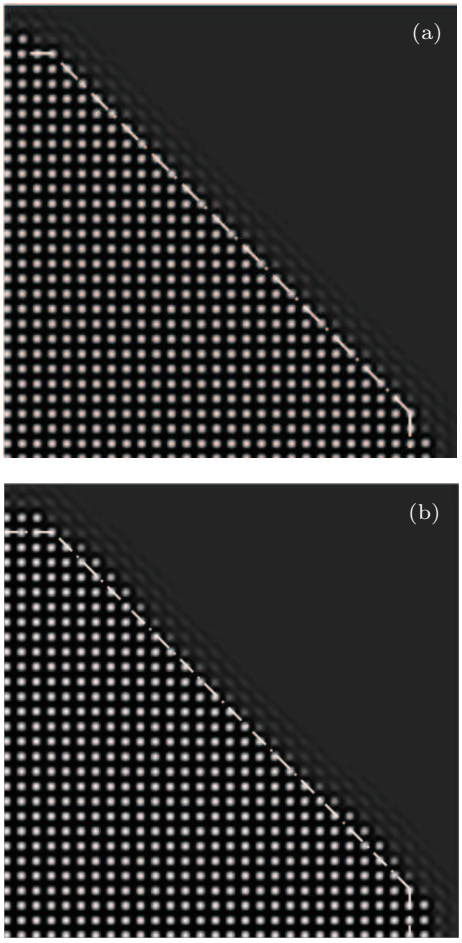


Fig. 5. Nucleation processes at {10} and {11} faces, simulated with $\bar{n} = -0.1$ and $\alpha_1 = 3$, at times: (a) $t = 1.08 \times 10^5$ and (b) $t = 1.11 \times 10^5$. For a better visualization, only a quarter of the simulation cell is displayed.

Lastly, figure 8 shows the diffusionless crystallization process simulated by parameters $\bar{n} = -0.06$ and $\alpha_1 = 2$. Compared with Figs. 2(a) and 2(b), the diffusionless crystallization mode is shown to exhibit a faster linear growth behavior, which is caused by a special interface migration mechanism, i.e., local atom rearrangement from the liquid state to the solid state.[8] As shown in Fig. 8(a), the interface associated with the diffusionless growth mode exhibits a low growth anisotropy arising from the orientation averaging of the interface accompanying its dynamic broadening. Due to its fast growth rate, the system is quickly occupied by a solid phase with no large density change as that of the initial liquid at time $t = 9.0 \times 10^3$, as shown in Fig. 8. Notably, this solid phase would eventually decompose into the two equilibrium phases driven by the remaining free energy difference ΔG_2. As shown in Fig. 1, although the driving force is lowered with the average density field decreasing from $\bar{n} = -0.05$ to $\bar{n} = -0.06$, which would favor the diffusive growth mode, the diffusionless crystallization still occurs when the peak width of correlation function becomes narrower. This results from the mutual interplays between interface type, crystallization mode, and correlation function. In Ref. [6], the diffusionless growth mode has been demonstrated to be coupled with the non-faceted interface. Moreover, the crystal–liquid interface would show more diffusive (non-faceting) behavior with a smaller peak width of correlation function according to Ref. [28], which is shown in Fig. 8(a). Therefore, it is expected that the diffusionless growth mode is more prone to be selected with a narrower peak width when the necessary thermodynamic condition is satisfied.

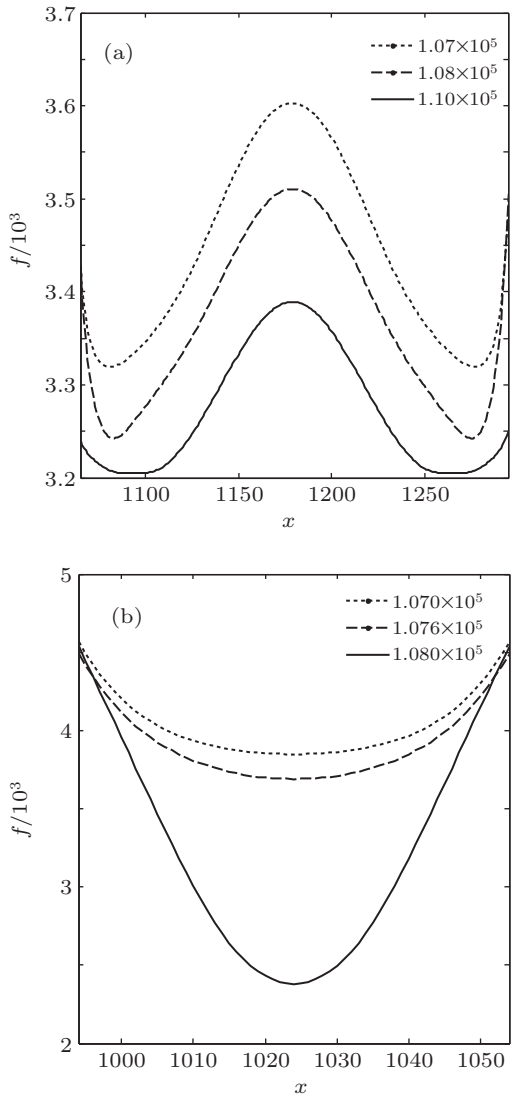


Fig. 6. The smooth free energy distributions along lines *CDE* (a) and *ABC* (b) before and during nucleation at the late growth stage, corresponding to Fig. 5.

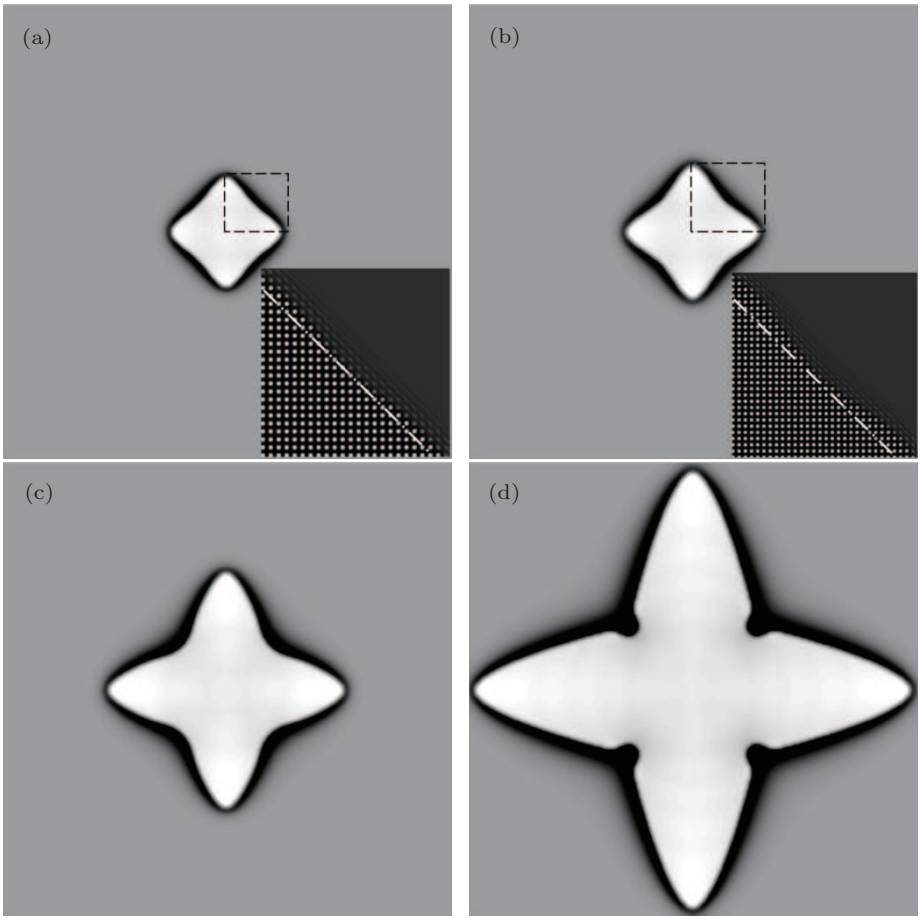


Fig. 7. The four-fold symmetric dendritic growth shown by the smoothed number density maps simulated with parameters $\bar{n} = -0.05$ and $\alpha_1 = 3$, at times: (a) $t = 3.5 \times 10^3$, (b) $t = 4.5 \times 10^3$, (c) $t = 9.0 \times 10^3$, and (d) $t = 1.8 \times 10^4$. The insets represent the corresponding number density field for the area enclosed by the black dashed box.

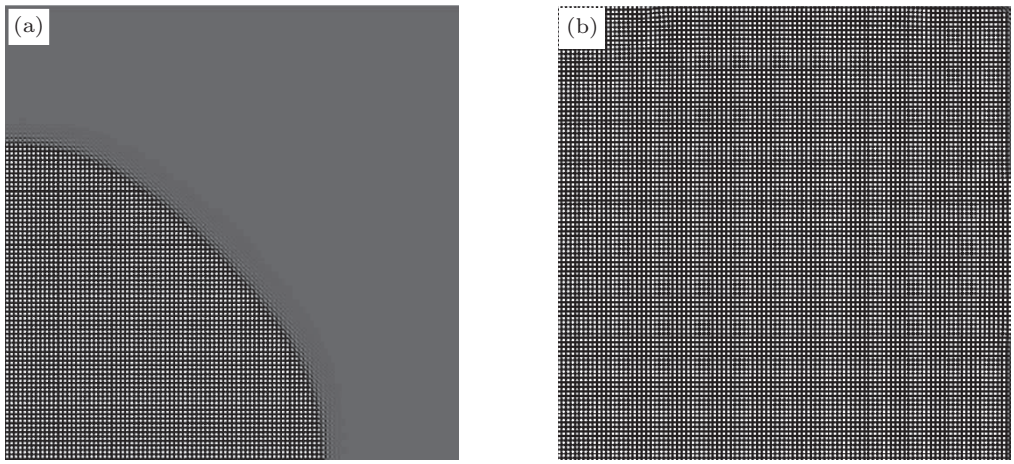


Fig. 8. The diffusionless crystallization process simulated with parameters $\bar{n} = -0.06$ and $\alpha_1 = 2$, at times: (a) $t = 4 \times 10^3$ and (b) $t = 9.0 \times 10^3$. For a better visualization, one quarter of the simulation cell is displayed.

4. Conclusions

In this paper, the crystallization process within the solid–liquid coexistence region governed by diffusion-controlled and diffusionless growth modes is investigated using the PFC method on an atomic scale. For the diffusionless growth mode to occur, the corresponding driving force should be greater than zero which dictates that the average density of the undercooled liquid should exceed the critical value where the two phases have the equal free energy. When the peak width of the correlation function becomes narrower, the diffusionless

crystallization mode is more favorable to be selected, owing to the symbiosis of the interface type and growth mode.[8] As for the diffusion-controlled regime, the orientation selection process during the growth of faceted square crystal is analyzed. The new $\{10\}$ layers tend to nucleate at the center of the plane, while the preferable nucleation sites for $\{11\}$ layers transit from the central area to positions near the corners of the truncated square, resulting from the non-uniform distribution of the supersaturation. Under a larger driving force obtained by increasing the average number density, the square crystal gradually loses its stability and evolves into the four-fold symmetric dendrite at a later time, caused by the relative reduction of incubation time with respect to that of growth.

References

[1] Gránásy L, Pusztai T, Börzsönyi T, Warren J A and Douglas J F 2004 *Nat. Mater.* **3** 645
[2] Taguchi K, Mayaji H, Izumi K, Hoshino A, Miyahoto Y and Kokawa R 2001 *Polymer* **42** 7443
[3] Beers K L, Douglas J F, Amis E J and Karim A 2003 *Langmuir* **19** 3935
[4] Xu H J, Matkar R and Kyu T 2005 *Phys. Rev. E* **72** 0110804
[5] Wild R and Harrowell P 2001 *J. Chem. Phys.* **114** 9059
[6] Russel W B, Chaikin P M, Zhu J, Meyer W V and Rogers R 1997 *Langmuir* **13** 3871
[7] Tegze G, Gránásy L, Tóth G I, Douglas J F and Tamas Pusztai 2011 *Soft Matter* **7** 1789
[8] Tegze G, Tóth G I and Gránásy L 2011 *Phys. Rev. Lett.* **106** 195502
[9] Cahn J W and Hilliard J E 1958 *J. Chem. Phys.* **28** 258
[10] Hillert M 1961 *Acta Metall.* **9** 525
[11] Wang Y Z and Li J 2010 *Acta Mater.* **58** 1212
[12] Boettinger W J, Warren J A, Beckermann C and Karma A 2002 *Ann. Rev. Mater. Res.* **32** 163
[13] Gao Y, Liu H, Zhou N, Xu Z, Zhu Y M, Nie J F and Wang Y 2012 *Acta Mater.* **60** 4819
[14] Chen L Q 2002 *Ann. Rev. Mater. Res.* **32** 113
[15] Zhou N, Shen C, Wagner M F X, Eggeler G, Mills M J and Wang Y 2010 *Acta Mater.* **58** 6685
[16] Lu Y, Wang C, Gao Y, Shi R, Liu X and Wang Y 2012 *Phys. Rev. Lett.* **109** 086101
[17] Gao Y, Zhou N, Yang F, Cui Y, Kovarik L, Hatcher N, Noebe R, Mill M J and Wang Y 2012 *Acta Mater.* **60** 1514
[18] Liu H, Gao Y, Liu J Z, Zhu Y M, Wang Y and Nie J F 2013 *Acta Mater.* **61** 453
[19] Elder K R, Katakowski M, Haataja M and Grant M 2002 *Phys. Rev. Lett.* **88** 245701
[20] Long J, Wang Z Y, Zhao Y L, Long Q H, Yang T and Chen Z 2013 *Acta Phys. Sin.* **62** 218101 (in Chinese)
[21] Gao Y J, Luo Z R, Huang C G, Lu Q H and Lin K 2013 *Acta Phys. Sin.* **62** 050507 (in Chinese)
[22] Yang T, Chen Z and Dong W P 2011 *Acta Metall. Sin.* **47** 1301
[23] Yang T, Chen Z, Zhang J, Dong W P and Wu L 2012 *Chin. Phys. Lett.* **29** 078103
[24] Tang S, Wang Z J, Guo Y L and Wang J C 2012 *Acta Mater.* **60** 5501
[25] Tang S, Backofen R, Wang J C, Zhou Y H, Voigt A and Yu Y M 2011 *J. Cryst. Growth* **334** 146
[26] Chen C, Chen Z, Zhang J, Yang T and Du X J 2012 *Chin. Phys. B* **21** 118103
[27] Greenwood M, Provatas N and Rottler J 2010 *Phys. Rev. Lett.* **105** 045702
[28] Greenwood M, Rottler J and Provatas N 2011 *Phys. Rev. E* **83** 031601
[29] Guo C, Wang Z J, Wang J C, Guo Y L and Tang S 2013 *Acta Phys. Sin.* **62** 108104 (in Chinese)
[30] Aaronson H I 2002 *Metall. Mater. Trans. A* **33** 2285
[31] Humadi H, Hoyt J J and Provatas N 2013 *Phys. Rev. E* **87** 022404
[32] Cherno A A 1974 *J. Cryst. Growth* **24/25** 11
[33] Yokoyama E and Kuroda T 1990 *Phys. Rev. A* **41** 2038